

# Analysis of the island effect for ELT MICADO MAORY SCAO mode

A. Bertrou-Cantou<sup>a\*</sup>, E. Gendron<sup>a</sup>, G. Rousset<sup>a</sup>, F. Vidal<sup>a</sup>, V. Deo<sup>a</sup>, and F. Ferreira<sup>a</sup>

<sup>a</sup>LESIA, Observatoire de Paris - CNRS - UPMC - Univ. Paris 7 Diderot  
5 place Jules Janssen, 92190 Meudon, France

## ABSTRACT

The presence of 51-cm wide spiders supporting the secondary mirror of the Extremely Large Telescope breaks the wave-front continuity of the incoming light and suggests to consider the telescope pupil as 6 independent petals, each of them having a different piston value. It is therefore necessary to co-phase them in order to return to a single continuous wave-front. Not being corrected, these phase steps in the pupil would severely decrease the optical performance. As part of MICADO instrument Single Conjugate Adaptive Optics (SCAO), a Pyramid wave-front Sensor (P-WFS) is being used to provide a measurement of the aberrated wave-front. Diffractive optics enables to describe phase steps across the pupil as a signal in the wave-front sensor focal plane: a piston applied on one of the 6 segments will create a specific pattern on the detector plane of the P-WFS so that it should - in principle - be possible to detect it. However, in practice, the sensor is not sensitive enough to differential piston due to other wave-front errors and it drives M4 to take unintended piston values on its six segments. This effect is known as petalling.

The adaptive optics end-to-end simulation platform COMPASS allows to perform numerical simulations in closed loop and quantify the impact of IE on the SCAO performance. Specifically, we investigate the P-WFS differential piston sensing capability under atmospheric turbulence, with remaining closed-loop residuals.

We show that these residuals are read as spurious differential piston : this error being additive throughout the time, the differential piston varies rapidly and reaches values up to a few microns. To cope with this effect, we set up a minimum mean-square error (MMSE) reconstructor dedicated to differential piston estimation control and we compare the results with the already implemented slaved actuators method.

**Keywords:** Adaptive Optics, Pyramid Wave-Front Sensor, Extremely Large Telescope, Differential Piston

## 1. INTRODUCTION

MICADO instrument Single Conjugate Adaptive Optics (SCAO) mode is based on a Pyramid wave-front Sensor (P-WFS) working in the visible, with the aim to work at the diffraction limit of the Extremely Large Telescope in the near infrared.<sup>1</sup> However, the P-WFS wave-front sensing capability is currently limited - among other things - by the presence of 51 cm-wide spiders, essential to support the telescope secondary mirror. They segment the incoming wave-front into 6 sub-wave-fronts, with different pistons that need to be co-phased.

The P-WFS proposed by Roberto Ragazzoni was first presented as a slope sensor<sup>2</sup> with promising performance. It is now thoroughly assessed and it is demonstrated to be more sensitive than the Shack-Hartmann wave-front sensor (Ragazzoni and Farinato<sup>3</sup> ; Esposito and Riccardi<sup>4</sup>). Another remarkable feature of this sensor is its phase step sensing capability : the light from both sides of the spiders is diffracted and interferes in a differential piston signal along and below these spiders. An expression of the pyramid signal as a function of a phase step in the pupil can be found in Esposito et al.<sup>5</sup> and a more detailed development of diffraction theory equations is proposed by Burvall et al.<sup>6</sup>

The use of the P-WFS for differential piston measurement was demonstrated in the context of segmented mirrors preliminary phasing and alignment,<sup>7</sup> and in emulated atmospheric turbulence using spatial filtering techniques and temporal averaging of the turbulence.<sup>8</sup> However, these methods do not apply to our case, where we need a fast measurement of both differential piston and full turbulent wave-front with the same sensor. This problematic was recently addressed in the framework of the HARMONI design phase by Schwartz et al.<sup>9</sup> under the name of

---

\* Corresponding author. E-mail: `arielle.bertrou` at `obspm` dot `fr`, Telephone: +33 (0) 1 45 07 77 86

Island Effect (IE).

This paper presents ongoing research to manage island effect in the context of the MICADO SCAO module on the ELT, at a sensing wavelength of 700 nm and under residual turbulence. Section 2 aims to quantify the impact of pupil segmentation due to large spiders on SCAO performance. In section 3, we give an explanation for the spurious and additive differential piston measurements provided by the pyramid. We come up with an alternative solution to deal with island effect, based on a minimum mean-square error (MMSE) reconstructor dedicated to petal piston estimation, which we develop in section 4.

## 2. QUANTIFICATION OF THE IMPACT OF SPIDERS ON OPTICAL PERFORMANCE

### 2.1 Simulation setup

The AO end-to-end simulation platform COMPASS allows to perform numerical simulations in closed loop with ELT-like conditions,<sup>10</sup> summarized in Table 1. The telescope pupil is dodecagonal with a diameter of 39 m, obscured by the secondary mirror and 6 spiders of 51 cm width. The deformable mirror (M4 in the ELT optical design) is made of 6 independent petals. Actuators are disposed in a hexagonal geometry and we use a total number of 4310 useful actuators. The pyramid WFS is working with a modulation of  $3\lambda/D$  and  $92 \times 92$  subapertures (detector pixels). Useful pixels follow the same geometry as the telescope pupil, i.e. some pixels below the spiders are not used. We use the slopes maps of the P-WFS and the mirror modes to build an interaction matrix (see Vidal et al.<sup>11</sup>). We typically filter 100 modes with the smallest eigenvalues in the least-square inversion process, and we obtain a command matrix referred to as "conventional" command matrix.

Table 1: Detailed simulation configuration.

Simulation configuration	
Telescope pupil	ELT like : $\varnothing = 39$ m with six 51cm wide spiders
Atmosphere	35 layers ESO Q3 : $r_0 = 12,9\text{cm}$ $L_0 = 25\text{m} - \ v\  = 10 \text{ m.s}^{-1}$
Deformable Mirror	M4 with 4310 actuators M5 Tip/Tilt
Pyramid WFS	$r_{mod} = 3\frac{\lambda}{D} - \lambda_{P-WFS} = 700\text{nm}$ $92 \times 92$ sub-apertures Mag 11
Target	$\lambda_{tar} = 2200\text{nm}$
Frame rate	500 Hz

### 2.2 Performance in the presence of spiders

In the closed loop simulation, COMPASS computes the residual wave-front at each iteration, from which we derive the mean phase value per segment : the segment piston  $P$ . The differential piston  $\Delta P$  is the difference between the piston value of a segment with respect to its clock-wise direct neighbour :  $\Delta P_i = P_{i+1} - P_i$  for  $i \in [0, 4]$ . The atmospheric turbulence induces natural phase steps between segments. To get a hint of the properties needed for the phasing sensor, we record  $\Delta P$  present in an uncompensated wave-front emulated by COMPASS following atmospheric turbulence statistics as defined in Table 1. The results are reported in Figure 1. The mean differential piston between segments is 793 nm, which is larger than our sensing wavelength and confronts us to the phase ambiguity problem (Pinna et al.<sup>12</sup>). It evolves at a mean rate of 11 nm/iteration at 500 Hz, meaning the differential phase correction should be achieved at a frequency rate of the order of the AO loop rate.

The 5 differential pistons obtained during a 2000 iterations conventional closed loop (blue, with left y-axis) are shown in Figure 2 with its associated long exposure Strehl Ratio computed at  $\lambda_{tar} = 2.2\mu\text{m}$  (red, with right y-axis). After a few iterations, the segment pistons start diverging, reaching tens of microns at the end, due to M4 bad command. These uncorrected phase steps have a severe implication regarding the Strehl ratio in the scientific instrument focal plane : it does not perform better than 15%, that is a fifth of the performance computed by Vidal et al. in the same conditions *without* spiders.<sup>11</sup> This performance reveals that our conventional

command law and the P-WFS are unable to clearly identify the differential piston, and it is consistent with the results of Schwartz et al.<sup>9</sup> for HARMONI design phase.

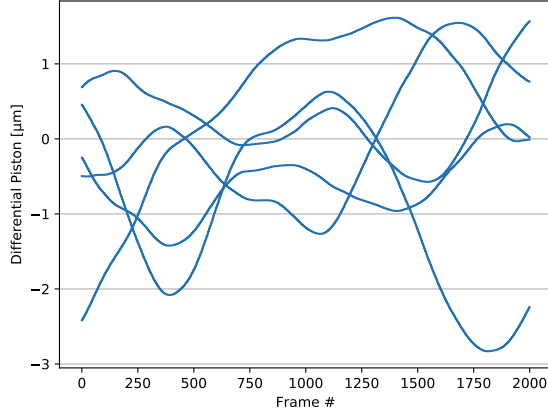


Figure 1: Evolution of the 5 natural differential pistons due to atmospheric turbulence and telescope pupil segmentation, with Table 1 parameters.

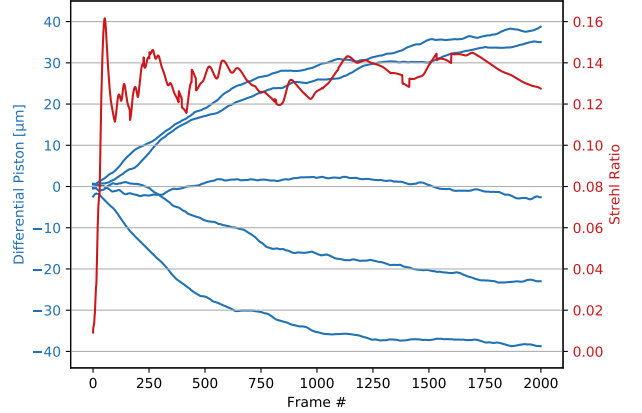


Figure 2: Drift of the differential pistons in the aperture due to the poor compensation by the conventional AO closed loop (blue, left y-axis). The related long exposure Strehl Ratio is shown in red (right y-axis).

### 3. THE UNMEASURABLE ISLAND EFFECT UNDER TURBULENCE WITH A PYRAMID

To this day, the pyramid in the visible on an ELT does not reach a perfect diffraction-limited correction and a realistic case study for  $\Delta P$  sensing should include the wave-front residuals of the adaptive optics closed-loop feeding the P-WFS. To thoroughly assess the ability of the P-WFS to sense differential piston under the ELT atmospheric turbulence, we take this partial correction regime into account with simulation conditions as specified in the previous section (see Table 1).

#### 3.1 Pyramid response to phase steps under partially corrected wave-front

It is well established that the presence of closed-loop residuals (including pyramid non linear effects and deformable mirror fitting error term) impacts the pyramid performance, leading to the emergence of compensation methods fighting against optical gain variations.<sup>13</sup> Figure 3 illustrates a typical residual wave-front obtained after convergence of a closed loop. The differential piston error was removed from the wave-front and its remaining error is composed of continuous modes - by continuous modes, we here refer to all modes except differential piston - resulting in a 162 nm RMS wave-front error.

The pyramid response to an increasing piston on one of its segment is studied in Figure 4. In a diffraction-limited regime, we find the sinusoidal,  $\lambda$  periodic, response as described in literature.<sup>5</sup> When a segment piston is measured together with a residual phase  $\phi_{res}$  (deprived from  $\Delta P$ ) (Figure 4, red curves - each curve being the response to a different petal), the response is dramatically affected from the calibrated one through three distinct impacts : a "flattened" response referring to the optical gain compensation problem, an offset along y-axis and thirdly, a dephasing. These errors constantly evolve with the nature of the residual phase upstream of the wave-front sensor. A predictive correction of this effects appears to be complex. The residuals-induced offset and gain prevent the loop from converging as the problem does not longer have a solution converging towards zero : we face a diverging system which errors are permanently integrated throughout time as seen in Figure 2. The figure also shows the response with an error phase  $\phi_{fit}$ , limited by a pure fitting error from the DM only, and not the P-WFS. As expected, it is characterized by a reduced sensitivity but the sinusoidal nature of a phasing sensor is preserved.

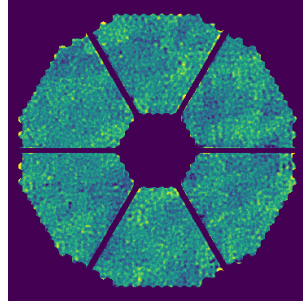


Figure 3: Wave-front residuals of a closed loop system on the ELT. Differential piston between petals has been removed here to show the structure of the residual phase.

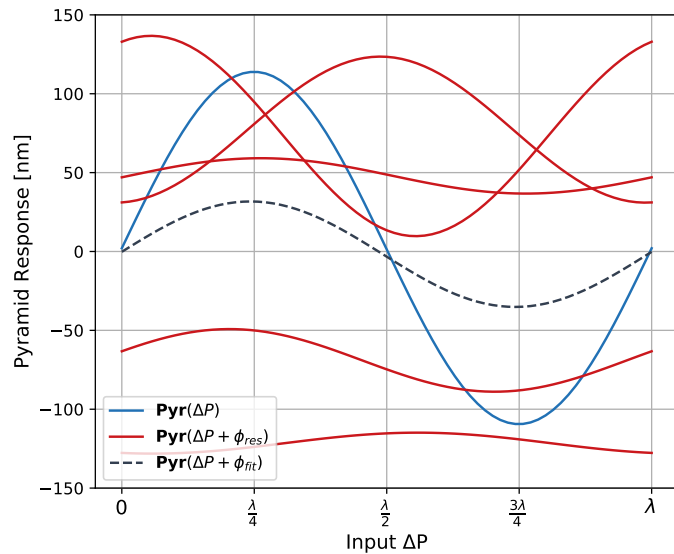


Figure 4: Pyramid WFS response to petal piston modes with and without the same residual wave-front  $\phi_{res}$

### 3.2 $\Delta P$ and continuous modes entanglement over time

The COMPASS simulation framework enables to work with an additional deformable mirror emulating phase steps in the segments : we call it the petal DM. It is used to perfectly correct for differential piston - which is traceable in the wave-front residuals computed by the simulation - independently from M4 and M5 Tip/Tilt DMs of the conventional closed-loop. This petal DM has a command matrix  $C_{petal}$  allowing to derive the pyramid measured  $\Delta P$ . Under the same atmospheric conditions, we can close the loop and record the differential piston measured by the pyramid over time with three different system scenarios :

- A conventional closed loop : M4 is controlled with a conventional command matrix as described in Section 2, without applying any other correction. The residuals contain a significant amount of  $\Delta P$  as shown in Figure 5a as well as other orders due to the non perfect pyramid behavior and the DM fitting term.
- A conventional closed loop assisted by an ideal theoretical petal correction: M4 is controlled in the same conventional way as in the previous case but in addition, a perfect petal DM compensates in a theoretical, perfect and instantaneous way any differential piston (see Figure 5b). This study reveals that the P-WFS still detects some differential piston when there is absolutely none.

- The third case is the "opposite" of the previous one : no turbulence nor residuals but only the segment pistons are present, as seen Figure 5c. It allows to know what  $\Delta P$  measurements the pyramid would provide in an open-loop system and in the absence of any wave-front residuals.

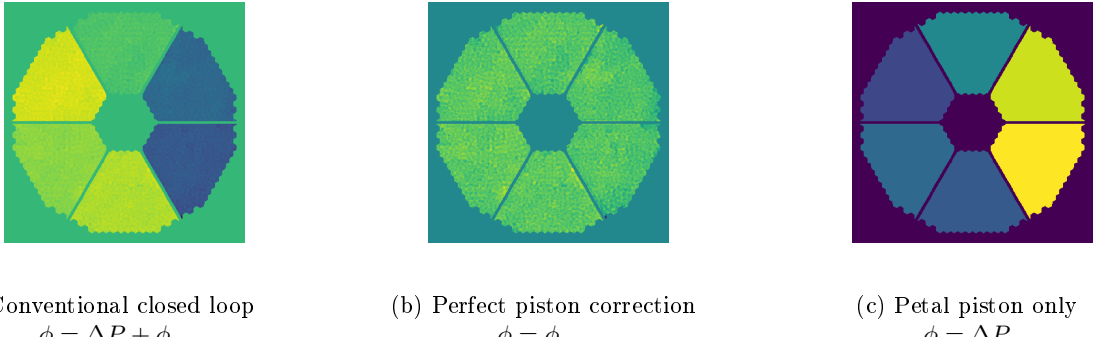


Figure 5: wave-front residuals seen by the pyramid for three simulated cases. The case (a) of a conventional closed loop introducing diverging pistons is composed into the phase residuals only (b) and the piston only (c)

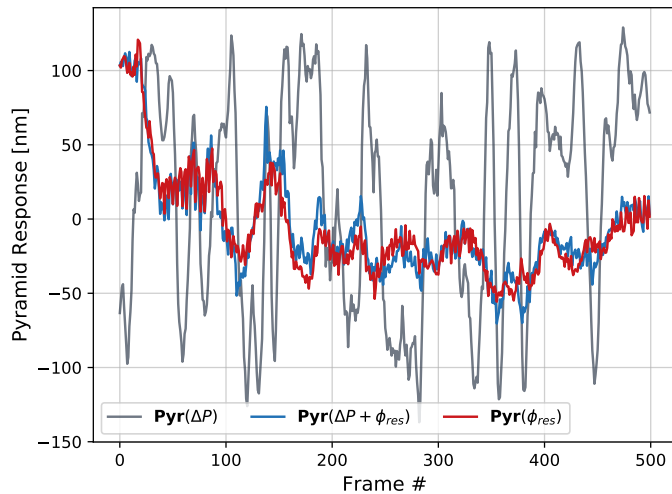


Figure 6: One of the 5 differential pistons measured by the pyramid in the three cases presented Fig. 5: a conventional closed loop system (blue) and in a closed loop system where segment pistons are perfectly removed with the petal DM (red). The gray curve shows an open-loop pyramid measurement of the differential piston actually present in the aperture, without any other wave-front residuals left.

Figure 6 shows one of the differential piston measured by the pyramid for 1 second in the three aforementioned cases. It stands out the pyramid still detects segment pistons when there is no segment piston left in the incoming wave-front (red curve). The response of the pyramid to the residuals with (blue) and without (red) presence of differential piston follow the same trend: this suggests the mismeasurement comes from a severe confusion between the true IE information from the wave-front residuals. In the pyramid measurement,  $\Delta P$  signal is generated by the AO continuous modes correction residuals. It confirms the results presented in the previous subsection and highlights it is persistent over time.

Finally, the open loop case with only petal pistons in the aperture (gray curve) shows that the pyramid measures and handles island effect with a sinusoidal behavior as described by Esposito et al.<sup>7</sup>: the rapid oscillations of the gray curve goes back to the rapid drifting of the differential piston (as seen in Fig.2) and to the theoreoretical

sinusoidal behavior of the phase step measurement. If we close the loop in these conditions, the  $\Delta P$  values would settle around multiples of  $\lambda_{P-WFS}$ .

## 4. DIFFERENTIAL PISTON HANDLING WITH MMSE METHOD

As seen in Section 3, the pyramid measurement and M4 control are adding spurious differential pistons to the wave-front residuals. In order to correct this effect, we want to estimate the value of the segment pistons introduced by based on the measurements of the other modes, using a Minimum Mean Square Error (MMSE) estimator. It means the control matrix will reconstruct the phase over the six independent petals and the MMSE estimator will provide the piston values to ensure the best wave-front continuity in order to match Kolmogorov statistics.

### 4.1 MMSE reconstructor implementation

A first step is to deprive the command of M4 from any  $\Delta P$ , so the only remaining petal pistons in the residuals are the natural ones, characterized in Figure 1. To do so, we introduce two matrix:

1.  $Petal_{M4}$  is a matrix that contains the 6 petals produced by M4 actuators
2.  $P_{actu}$  is the matrix giving the 6 piston values produced by each actuators.

The command matrix that make the deformable mirror "flat" in terms of segment piston is:

$$C' = (Id - Petal_{M4}P_{actu})C_{nom} \quad (1)$$

$C_{nom}$  is the conventional command matrix, as defined in Section 2. The remaining differential piston is the atmospheric contribution and follows Kolmogorov's law. The residual error in the measurement is the difference between the true atmospheric piston value  $p_{atm}$  and the reconstructed one  $\mathbf{R}u$  from the actuator voltages  $u$ , deprived of differential piston, as stated above. The minimum mean-square error (MMSE) differential piston reconstructor  $\mathbf{R}$  that minimizes  $\langle \|p_{atm} - \mathbf{R}u\|^2 \rangle$  is defined by:

$$\mathbf{R} = cov_{p_{atm}u}cov_{uu}^{-1} \quad (2)$$

where  $cov_{xy}$  is the turbulence covariance matrix of  $x$  and  $y$ . Finally, we have the new command matrix handling island effect:

$$C = (1 + Petal_{M4}\mathbf{R})(1 - Petal_{M4}P_{actu})C_{nom} \quad (3)$$

In addition, we apply a low-pass filter to this command with a gain  $\gamma$  to smooth the M4 response to piston control, as shown in the block diagram of Figure 7. We consider the control vector  $v_k$  of the actuators voltages to be applied to M4 and a state vector  $p_k$  containing the piston values applied on each segment. We use the 2 matrices generic controller of COMPASS which allows to implement our command law and from (3) we get:

$$\begin{aligned} \begin{pmatrix} v_k \\ p_k \end{pmatrix} &= E \begin{pmatrix} v_{k-1} \\ p_{k-1} \end{pmatrix} + C m_k \\ &= \begin{pmatrix} Id & -(1-\gamma)Petal_{M4} \\ 0 & (1-\gamma)Id \end{pmatrix} \begin{pmatrix} v_{k-1} \\ p_{k-1} \end{pmatrix} - \begin{pmatrix} (1+\gamma Petal_{M4}\mathbf{R})(1-Petal_{M4}P_{actu})C_{nom} \\ -\gamma\mathbf{R}(1-Petal_{M4}P_{actu})C_{nom} \end{pmatrix} m_k \end{aligned}$$

where  $m_k$  denotes the measurements provided by the wave-front sensor.

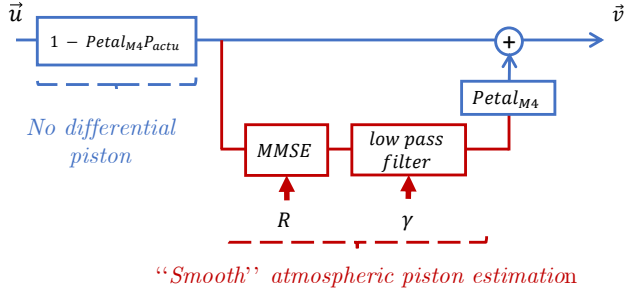


Figure 7: MMSE command loop block diagram for piston segment control.

## 4.2 Results

With this new command law and an optimized  $\gamma$  factor ( $\gamma = 0.05$ ), we perform simulations and report the long exposures Strehl Ratio (LESR) in K-band over 2000 iterations in Figure 8. For comparison, we also implemented the slaved actuators method introduced by Schwartz et al,<sup>9</sup> imposing the same control value to actuators located on each side of the spiders. The best performance with no island effect (ideal compensation od differential piston) is 82% of long exposure Strehl ratio, shown in the top green curve on Fig. 8. Note that it should stays flat at 82 % but it unexpectedly slowly decreases because of local problem in that particular simulation, that we shall ignore here. At the opposite of that perfect case, the worst one is when running the simulation without applying any dedicated piston correction, the closed loop system provides a LESR of 16%. The MMSE reconstructor we implemented provides a clear improvement. An exemple of wave-front residuals obtained with this method is shown in Figure 9. However, the LESR of 58% is not yet fully satisfactory and lower than the 68% achieved with the slaved actuators method.

## CONCLUSIONS & PERSPECTIVES

The pupil segmentation of the ELT due to a six-legged spider breaks the spatial continuity of the incoming wave-front. The latter is hence seen as 6 independent sub-wave-fronts and the differential piston naturally present between each segment, called island effect, needs to be corrected. Unlike phasing and alignment of the ELT primary mirror segments, relying on active optics, island effect is an issue which has to be tackled at a rapid rate and should be considered as an integral part of the adaptive optics system. The pyramid wave-front sensor is sensitive to this effect, but only under favorable conditions, when correction is closed to diffraction. Under MICADO-MAORY baseline case study with  $\frac{D}{r_0} > 300$ , the pyramid is poorly sensitive and this dramatically affects the Strehl ratio performance. In a worst case, the 6 segments are incoherent and the ELT is reduced to a sixth of its capability. In this paper, we have shown that this spurious behavior is related to the pyramid working too far from the diffraction-limited correction regime: the pyramid response to phase steps in the pupil in this regime significantly differs from the calibrated one and leads to a diverging system regarding island effect correction. This mismeasurement is related to a confusion between differential piston modes and other ones and it persist throughout time. We also show that efforts to enable the pyramid to work at the diffraction regime, and hence to get an AO system only limited by the deformable mirror geometry, would address this problem. In the second instance, we developed a minimum mean square reconstructor to estimate the value of the segment pistons. It relies on the measurement of the modes to infer the piston value each segment shoud take to follow Kolmogorov law of turbulence. While improved, the performance are not yet satisfactory and the slaved method appears to be better suited for island effect. However, none of these methods would be efficient to compensate for the apparition of non-Kolmogorov, non-turbulent segment pistons such as drifts in the reference body of M4 or local pistons induced by *low wind effect* as seen on SPHERE instrument on the VLT<sup>14</sup> because they require injection of petal discontinuities in the DM command to be compensated.

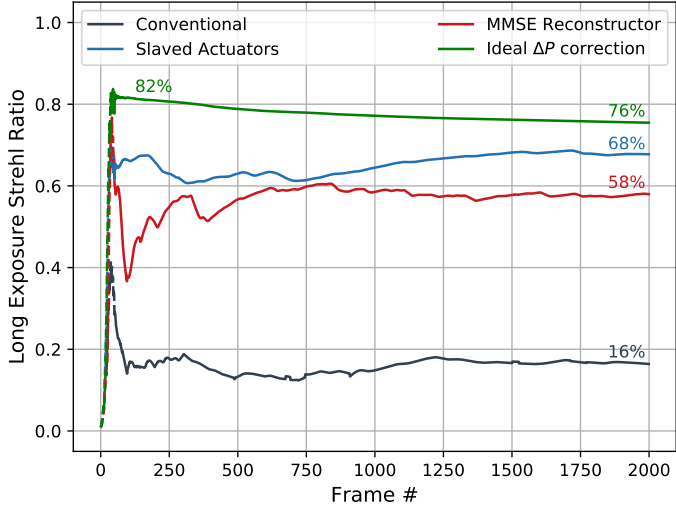


Figure 8: Evolution of long exposure Strehl Ratio (starting the average after closed-loop convergence at 50 it.) in the case of uncontrolled segment pistons (grey), MMSE control of differential piston (red) and with slaved actuators (blue). For comparison, the green curve shows the SR found with an ideal differential piston correction (green).

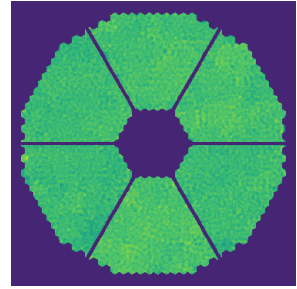


Figure 9: Residual phase of a MMSE reconstructor closed-loop with 167nm error RMS : 81 nm RMS contribution of  $\Delta P$  and 147nm RMS of other residuals.

## REFERENCES

- [1] Clénet, Y., Buey, T., Gendron, E., Hubert, Z., Vidal, F., Cohen, M., Chapron, F., Sevin, A., Férou, P., Barbary, G., Baudouz, P., Borgo, B., Nejma, S. B., Chamouleyron, V., Deo, V., Dupuis, O., Durand, S., Ferreira, F., Gaudemard, J., Gratadour, D., Huby, E., Huet, J.-M., Ruyet, B. L., Nguyen-Tuong, N., Perrot, C., Thijs, S., Younès, Y., Rousset, G., Feautrier, P., Zins, G., Diolaiti, E., Ciliegi, P., Esposito, S., Busoni, L., Schubert, J., Hartl, M., Hörmann, V., and Davies, R., “The MICADO first-light imager for the ELT: towards the preliminary design review of the MICADO-MAORY SCAO,” *Proc. SPIE* **10703**, 10703 – 10703 – 11 (2018).
- [2] Ragazzoni, R., “Pupil plane wavefront sensing with an oscillating prism,” *J. Mod. Opt.* **43**(2), 289–293 (1996).
- [3] Ragazzoni, R. and Farinato, J., “Sensitivity of a pyramidal wave front sensor in closed loop adaptive optics,” *Astronomy & Astrophysics* **350**, L23–L26 (1999).
- [4] Esposito, S. and Riccardi, A., “Pyramid wavefront sensor behavior in partial correction adaptive optic systems,” *Astronomy & Astrophysics* **369**, L9–L12 (Apr. 2001).
- [5] Esposito, S., Feeney, O., and Riccardi, A., “Laboratory test of a pyramid wavefront sensor,” *Proc. SPIE* **4007**, 416–422 (2000).
- [6] Burvall, A., Daly, E., Chamot, S. R., and Dainty, C., “Linearity of the pyramid wavefront sensor,” *Opt. Express* **14**(25), 11925–11934 (2006).
- [7] Esposito, S. and Devaney, N., “Segmented telescopes co-phasing using a pyramid sensor,” in [*Beyond conventional adaptive optics, ESO Conference and Workshop Proceedings*], 161 (2002).
- [8] Pinna, E., Quiros-Pacheco, F., Esposito, S., Puglisi, A., and Stefanini, P., “Signal spatial filtering for co-phasing in seeing-limited conditions,” *J. Opt. Soc. Am. A* **32**(23), 3465–3467 (2007).
- [9] Schwartz, N., Sauvage, J.-F., Correia, C., Petit, C., Quiros-Pacheco, F., Fusco, T., Dohlen, K., El Hadi, K., Thatte, N., Clarke, F., Paufique, J., and Vernet, J., “Sensing and control of segmented mirrors with a pyramid wavefront sensor in the presence of spiders,” *arXiv e-prints* , arXiv:1809.08839 (2018).

- [10] Ferreira, F., Gratadour, D., Sevin, A., Doucet, N., Vidal, F., Deo, V., and Gendron, E., “Real-time end-to-end AO simulations at ELT scale on multiple GPUs with the COMPASS platform,” *Proc. SPIE* **10703**, 1070347 (2018).
- [11] Vidal, F., Ferreira, F., Deo, V., Sevin, A., Gendron, E., Clénet, Y., Durand, S., Gratadour, D., Doucet, N., Rousset, G., and Davies, R., “End-to-end simulations for the MICADO-MAORY SCAO mode,” in [*5<sup>th</sup> AO4ELT conference-Adaptive Optics for Extremely Large Telescopes*], (2017).
- [12] Pinna, E., Esposito, S., Puglisi, A., Pieralli, F., Myers, R., Busoni, L., Tozzi, A., and Stefanini, P., “Phase ambiguity solution with the Pyramid Phasing Sensor,” *Proc. SPIE* **6267** (2006).
- [13] Deo, V., Gendron, E., Rousset, G., Vidal, F., Sevin, A., Ferreira, F., Gratadour, D., and Buey, T., “A telescope-ready approach for modal compensation of pyramid wavefront sensor optical gain,” *In review* (2019).
- [14] Milli, J., Kasper, M., Bourget, P., Pannetier, C., Mouillet, D., Sauvage, J.-F., Reyes, C., Fusco, T., Cantalloube, F., Tristram, K., Wahhaj, Z., Beuzit, J.-L., Girard, J., Mawet, D., Telle, A., Vigan, A., and N'Diaye, M., “Low Wind Effect on VLT/SPHERE : impact, mitigation strategy, and results,” *Proc. SPIE* **10703** (2018).